2D Materials

PAPER

RECEIVED
12 January 2017

REVISED
8 March 2017

ACCEPTED FOR PUBLICATION
16 March 2017

PUBLISHED
3 April 2017

Amorphous two-dimensional black phosphorus with exceptional photocarrier transport properties

Matthew Z Bellus[1,3], Zhibin Yang[2,3], Jianhua Hao[2], Shu Ping Lau[2] and Hui Zhao[1]

[1] Department of Physics and Astronomy, The University of Kansas, Lawrence, Kansas 66045, United States of America
[2] Department of Applied Physics, The Hong Kong Polytechnic University, Hung Hom Kowloon, Hong Kong, People's Republic of China
[3] These authors contributed equally to this work.

E-mail: huizhao@ku.edu **and** apsplau@polyu.edu.hk

Keywords: black phosphorus, amorphous, photocarrier, diffusion, mobility

Abstract

Recently, two-dimensional materials have been extensively studied. Due to the reduced dielectric screening and confinement of electrons in two dimensions, these materials show dramatically different electronic and optical properties from their bulk counterparts. So far, studies on two-dimensional materials have mainly focused on crystalline materials. Here we report studies of atomically thin amorphous black phosphorus, as the first two-dimensional amorphous material. Spatially and temporally resolved pump-probe measurements show that large-area and uniform atomic layers of amorphous black phosphorus, synthesized at low temperature, possess a long exciton lifetime of about 400 ps, a room-temperature exciton diffusion coefficient of 5 $cm^2 s^{-1}$, which is at least two orders of magnitude larger than amorphous silicon, and an exciton mobility of about 200 $cm^2 V^{-1} s^{-1}$. We also deduce from these values an exciton mean free time of 50 fs, a mean free path of 5 nm, and a diffusion length of 450 nm. These results suggest that amorphous black phosphorus can be potentially used in low-cost optoelectronic devices.

1. Introduction

Amorphous solids are an important type of material. In such noncrystalline solids, the arrangement of atoms has no long-range order. The absence of periodicity usually results in electronic states with fuzzy boundaries, allowing them to possess properties that are distinctly different from their crystalline counterparts. Furthermore, fabrication of amorphous materials is of low cost, making them attractive for many applications. For example, amorphous silicon dioxide is used as the gate dielectric in the silicon electronics industry. Amorphous silicon is widely used as an active layer in photovoltaic devices [1] and thin-film transistors [2]. Transparent thin-film transistors with mobilities exceeding 10 $cm^2 V^{-1} s^{-1}$ fabricated with amorphous In–Ga–Zn–O has been reported [3]. Tin-based amorphous oxides have been used for high capacity lithium-ion-storage [4]. Amorphous iron can be used as a catalyst for the hydrogenation of carbon monoxide [5], while amorphous metal-oxide films can serve as an oxygen evolution reaction catalyst [6].

So far, studies of amorphous solids have mostly focused on bulk materials. Recent developments in the research of two-dimensional (2D) crystals have revealed that these atomically thin materials can have significantly different properties from their 3D counterparts, offering a new way to develop functional materials [7–10]. Since the origin of these major differences, like the confinement of electrons in 2D systems and the lack of dielectric scattering of the Coulomb interactions, are not unique to crystalline materials, it is interesting to investigate 2D amorphous materials.

Here we report a study on photocarrier properties in amorphous black phosphorus (a-BP) atomic layers. Recently, BP has gained significant interest as a new 2D material [11]. Much of this attention has been drawn by its layered 2D nature when synthesized in its crystalline form, making it viable for many of the potential van der Waals crystal applications. Ultrathin and even monolayer BP, known as phosphorene, has been successfully fabricated from bulk crystalline BP [12] and has shown novel quantum confinement effects [13, 14]. Several studies have shown that [12, 15–18] the energy band gap of BP increases dramatically from the bulk value of 0.35 eV as the thickness approaches the monolayer limit, making it an attractive material for optical applications [19, 20]. Previous studies have also shown superior charge transport properties in ultrathin BP films [12,

21–29]. However, these studies are all focused on crystalline BP. In 2015, some of us, along with co-workers, reported the first successful fabrication of amorphous black phosphorus (a-BP) ultrathin films [30]. Wafer scale a-BP ultrathin films were fabricated by pulsed laser deposition (PLD) at low temperature [30]. Field effect transistors fabricated with 2 nm films show field effect mobilities of 14 $cm^2 V^{-1} s^{-1}$ and on/off ratios of about 100, revealing the potential applications of this material for thin-film transistors.

In this work, we show that large-area and uniform atomic layers of amorphous black phosphorus, synthesized at low temperature, have a high exciton diffusion coefficient and a long exciton lifetime. Temporally and spatially resolved pump-probe measurements revealed that in 2 nm a-BP ultrathin films excitons have a diffusion coefficient of about 5 $cm^2 s^{-1}$, which is at least two orders of magnitude larger than amorphous silicon, a long exciton lifetime of about 400 ps, and a long exciton diffusion length of about 450 nm. These results suggest potential applications of this material for low-cost optoelectronic devices.

2. Sample fabrication and characterizations

Amorphous black phosphorus ultrathin films were synthesized on Si substrates with a 300 nm oxide layer by PLD. A black phosphorus crystal (smart-element) was used as the target. The growth temperature was set at 150 °C and the base pressure of the chamber was evacuated to around 1.5×10^{-7} Torr. Three samples were fabricated, with nominal thicknesses of 2, 5, and 10 nm, according to previously established relation between the film thickness and the synthesis conditions [30]. Due to the instability of BP in air, a thin layer of poly(methyl methacrylate) (PMMA) was applied to protect the a-BP films.

The structure of the as-grown films was characterized by transmission electron microscopy (TEM) and x-ray diffraction (XRD). From the energy-dispersive x-ray spectroscopy (EDX) results shown in figure 1(a), the chemical composition of pure phosphorus (P) was confirmed. The minor peaks of copper (Cu) are attributed to the TEM grid. The amorphous nature of the samples was indicated by the high-resolution TEM (HRTEM) and XRD as illustrated in figures 1(b) and (c) respectively. These samples were named as amorphous BP, instead of amorphous phosphorous, because their short-range order of the lattice and their physical properties are close to BP, instead of other forms of phosphorous. Most recently, another amorphous phase of phosphorous, amorphous red phosphorus, was reported [31].

The films were further characterized by Raman spectroscopy. As shown in figure 1(d), three BP characteristic peaks were observed in the Raman spectra of the a-BP thin films with the nominal thicknesses of 2, 5, and 10 nm. As the thickness decreases, the peaks become broader and the intensity decreases significantly. For the 2 nm thick sample, the Raman peaks exhibit a shift of about 5 cm^{-1} with respect to the thicker films, which is consistent with the previous report [30]. This can be attributed to the consideration that for ultrathin films, the vibrational modes are more easily influenced by the highly disordered structure. Finally, the optical properties of the films were characterized. The room temperature photoluminescence (PL) spectrum of the 2 nm a-BP film is shown in figure 1(e). A 1.53 eV continuous-wave laser beam was used as the excitation source. The emission peak is located at 0.85 eV, which is attributed to the optical band gap of 2 nm a-BP. No PL was observed from the thicker films, suggesting that their optical band gaps are not in this spectral range. We note that since the films are covered by PMMA layers, their actual thickness cannot be confirmed by atomic force microscopy. However, both PL and Raman spectra confirms the 2 nm thickness of the thinnest sample.

3. Results and discussion

Transient reflection measurements [32] were performed to investigate photocarrier dynamics in the a-BP samples at room temperature. We will mainly focus on the 2 nm film. Figure 2(a) illustrates the pump-probe scheme of the measurement. The sample was excited by a 100 fs pump pulse with a photon energy of 1.57 eV, which is obtained from a Ti:sapphire laser. The probe pulse is obtained from an optical parametric oscillator that is pumped by the Ti:sapphire laser. The probe photon energy is 0.80 eV, which is tuned to near the optical band gap of the sample in order to effectively sense the reflectance change of the sample induced by the pump-injected photocarriers. Both the pump and probe are tightly focused on the sample by a microscope objective lens. Differential reflection of the probe was measured by lock-in techniques to monitor the photocarrier dynamics [32]. The differential reflection is defined as, $\Delta R/R_0 = (R - R_0)/R_0$, where R and R_0 are the reflection of the probe pulse with and without the presence of the pump, respectively. Measuring the differential reflection over different relative delay times between the pump and probe pulses allows us to time resolve the dynamics of the injected photocarriers. Figures 2(b) and (c) show the observed differential reflection signal, in short and long time ranges, respectively, with various values of pump fluence. We found that the signals reach their peaks on an ultrafast time scale, and then decay exponentially.

To understand the observed features, we first establish the relation between the signal and the photocarrier density. Figure 2(d) shows the peak signal as a function of the pump fluence, which is nearly proportional to the injected photocarrier density. Below 50 $\mu J\ cm^{-2}$, the differential reflection is approximately proportional to the pump fluence, and thus is proportional to the photocarrier density. A saturation effect can be seen at fluences higher than 50 $\mu J\ cm^{-2}$. The fluence

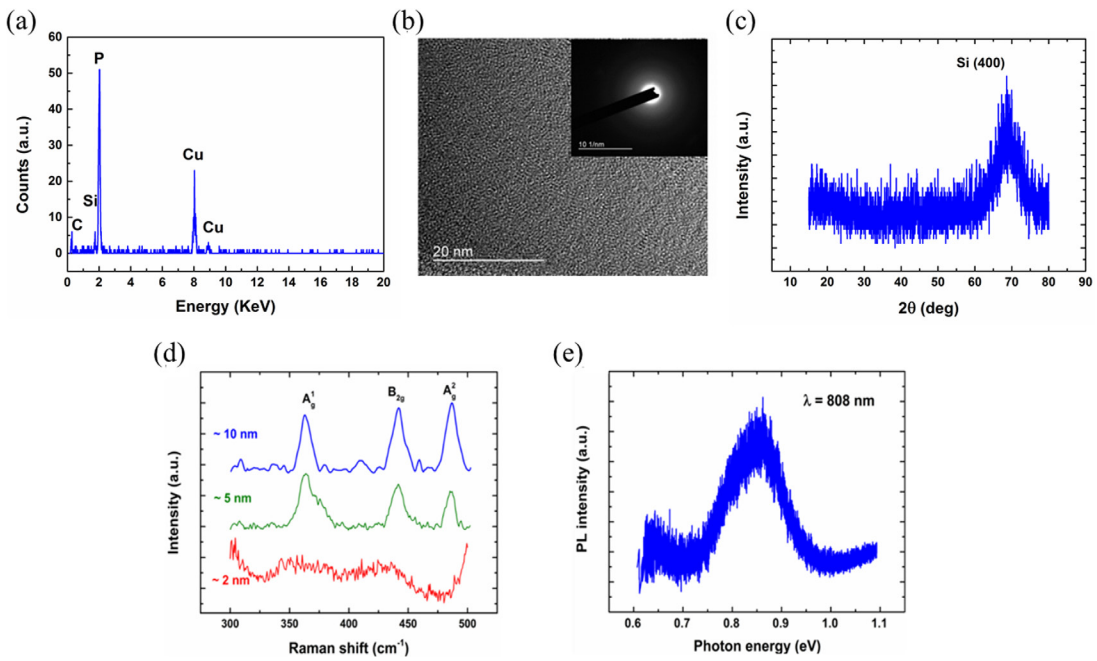

Figure 1. Structural characterization and optical properties of the a-BP thin films. (a) EDX spectrum of the a-BP thin films, confirming that pure phosphorus films were obtained. (b) High-resolution TEM image of the 10 nm a-BP film, combining the SAED pattern shown inset, revealing the highly disordered feature of the obtained films. (c) XRD pattern of the a-BP film grown on SiO_2/Si substrate. The only emerged peak is Si (400), further confirming the amorphous nature of the BP film. (d) Raman spectra of the a-BP thin films with different thicknesses. (e) PL spectrum of the 2 nm a-BP film under the excitation of an 808 nm laser.

dependence was fit by a standard saturation model, $\Delta R/R_0 \propto F/(F + F_{sat})$, where F_{sat} is the saturation fluence, which was found to be 120 μJ cm^{-2}.

With an excess energy of 0.72 eV, the pump pulse injected free electron–hole pairs with high kinetic energy. As shown in figure 2(b), the signal reaches the peak on an ultrafast time scale, even though the probe is tuned to near the optical band gap. The rising part of the signal can be modeled by the integral of a Gaussian function with a full width of 0.45 ps, which is slightly longer than the cross-correlation width of the pump and probe pulses of 0.35 ps. To understand this fast rising of the signal, we note that the initially injected nonequilibrium distributions of the electrons and holes are expected to undergo a thermalization process first, in which a thermal distribution is established via electron–electron and hole–hole scattering. This process is followed by an energy relaxation process via carrier-phonon scattering, in which these hot carriers cool down to the lattice temperature of 300 K. Both processes increase the population of carriers in the probed states near the band edge, and hence are expected to cause an increase of the signal. The observed ultrafast rising time hence suggests that these processes occur on sub-picosecond time scales in the a-BP ultrathin film. Ultrafast thermalization and energy relaxation of hot carriers have been observed in other 2D materials, such as transition metal dichalcogenides [32, 33] and graphene [34, 35], which can be attributed to the enhanced carrier–carrier and carrier-phonon interactions due to the reduced dielectric screening effect. Since this enhancement also exists in ultrathin a-BP, it is reasonable that these processes occur on a similar time scale. On the other hand, carrier thermalization and relaxation can take several tens of picoseconds in bulk semiconductors and quantum wells [36].

The decay of the signal can be fit by double exponential functions, $\Delta R/R_0(t) = A_1\exp(-t/t_1) + A_2\exp(-t/t_2) + B$, with two time constants t_1 and t_2. Least-square-fits were performed with A_1, A_2, B, t_1 and t_2 as fitting parameters. The fitting results are shown by the solid curves in figures 2(b) and (c). The two time constants are plotted as a function of the pump fluence in figure 2(e). Both time constants are independent of the pump fluence (i.e. injected carrier density) below 50 μJ cm^{-2}. The fast time constant of about 3 ps could be attributed to exciton formation. Due to the enhanced coulomb interaction between electrons and holes in this 2D system, the exciton binding energy is expected to be large, and excitons should be stable at room temperature. Ultrafast exciton formation from nonresonantly excited electron–hole pairs has been observed in monolayer transition metal dichalcogenides, as a fast decay of the transient reflection signal shorter than 1 ps [37, 38]. After this short transient, the rest of the decay can be described by a time constant of about 400 $\pm$ 20 ps, which is attributed to the exciton lifetime. We note that the longer time constants at high pump fluences could be attributed to the nonlinear dependence of the signal on the carrier density, as shown in figure 2(d). In that regime, the time evolution of the differential reflection signal does not accurately reflect that of the carrier density.

It is interesting to note that even in the saturation regime, there is no sign of exciton–exciton annihilation. Previous studies have shown that exciton–exciton

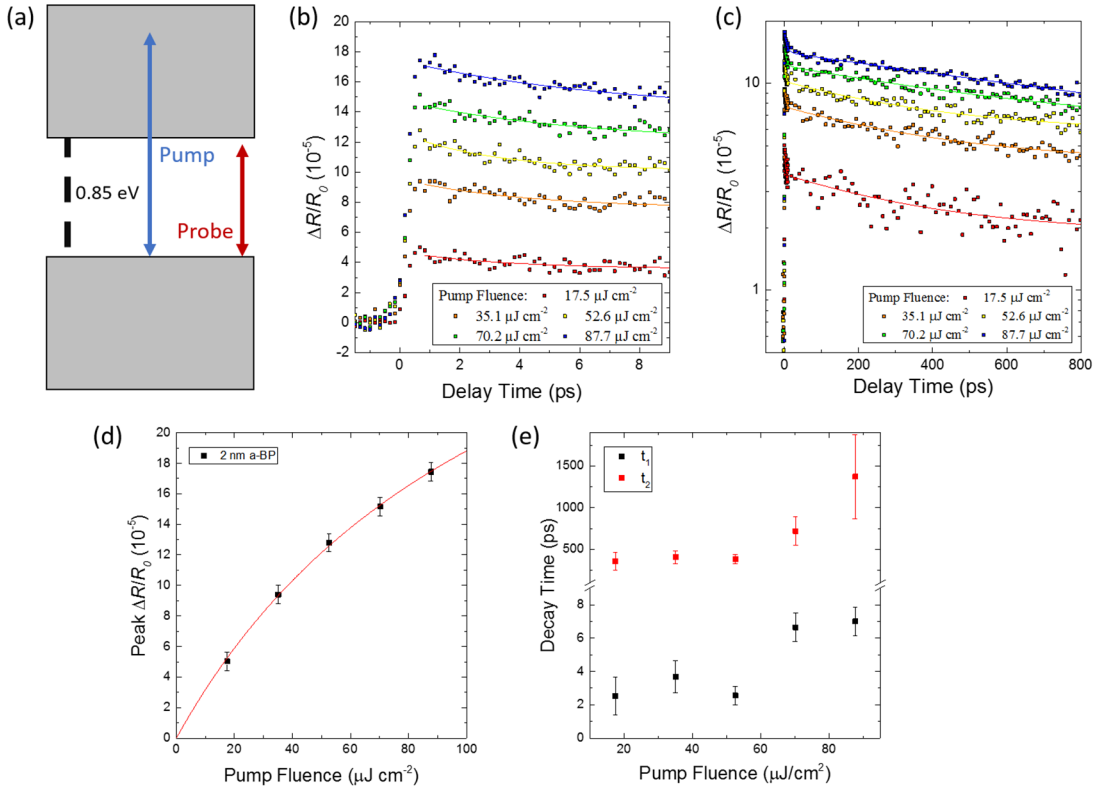

Figure 2. Differential reflection of the 2 nm a-BP ultrathin film. (a) Schematics of pump and probe scheme with respect to the electronic bands of the 2 nm a-BP film. (b) Differential reflection of the 2 nm a-BP film for different values of pump fluence. (c) Same as (b), but on a larger time range and in semi-logarithm scale (d) Peak $\Delta R/R_0$ signal as a function of pump fluence. The solid line shows a fit (see text). (e) The decay times, t_1 (black) and t_2 (red), obtained from from double exponential fits of the data in (c) as a function of pump fluence.

annihilation dominates dynamics of high density exciton populations in 2D TMDs [39–42]. In our measurement, the injected exciton density is comparable to the saturation density, as evident by the sub-linear power dependence shown in figure 2(d). In this regime, exciton–exciton scattering could cause faster decay of exciton population at higher density, which is not observed in figure 2(c). The absence of exciton–exciton annihilation is beneficial for applications involving a high-density of photocarriers. However, the mechanism of this effect is unclear.

To study the transport properties of excitons in a-BP, we performed spatially resolved differential reflection measurements. Using the focused 1.57 eV pump pulse, we injected carriers in the a-BP sample with a Gaussian profile of 2.5 μm full width at half maximum, which defined the spatial resolution of the study. Due to the induced density gradient, excitons diffuse two dimensionally. We do not consider a three dimensional diffusion as the sample is thinner than the injection depth of the lasers and thus photocarriers are injected throughout the sample thickness and diffuse in a planar direction. We then measured the differential reflection as a function of both probe position and probe delay relative to the pump.

The result of this spatiotemporal measurement is shown in figure 3(a). Here the probe position is defined as the distance between the centers of the pump and probe spots. As the excitons diffuse, the spatial Gaussian profile can be seen to expand, showing a clear sign of diffusive transport. Figure 3(b) shows the Gaussian profiles for several probe delays. Each profile was fit with a Gaussian function to extract its full width at half maximum. The squared width, w^2, is plotted as a function of the probe delay in figure 3(c). In the diffusion process with an initial Gaussian density profile, the width of the profile expands as $w^2 = w_0^2 + 11.09Dt$, where w_0 is the initial width and D, the diffusion coefficient of the excitons [32]. With a linear fit to the squared widths in figure 3(c), we find a diffusion coefficient of about $5.3 \pm 0.5\,\mathrm{cm^2\,s^{-1}}$. We note that the measurement was repeated at several locations of the sample and similar results were obtained.

The exciton diffusion coefficient obtained is significantly larger than other amorphous semiconductors. For example, in amorphous silicon, the most widely used amorphous semiconductor, the photocarrier diffusion coefficient is on the order of 0.01 to $0.001\,\mathrm{cm^2\,s^{-1}}$ [43–46]. Exciton diffusion is a thermal motion process limited by scattering. Hence, the diffusion coefficient reveals the microscopic interaction of excitons with their environment. Considering a room temperature thermal speed, v, of about $10^5\,\mathrm{m\,s^{-1}}$, the measured diffusion coefficient indicates a mean free time of $D/v^2 \approx 50$ fs, or a momentum relaxation rate of $2 \times 10^{13}\,\mathrm{s^{-1}}$, and a mean free path of 5 nm. Further-

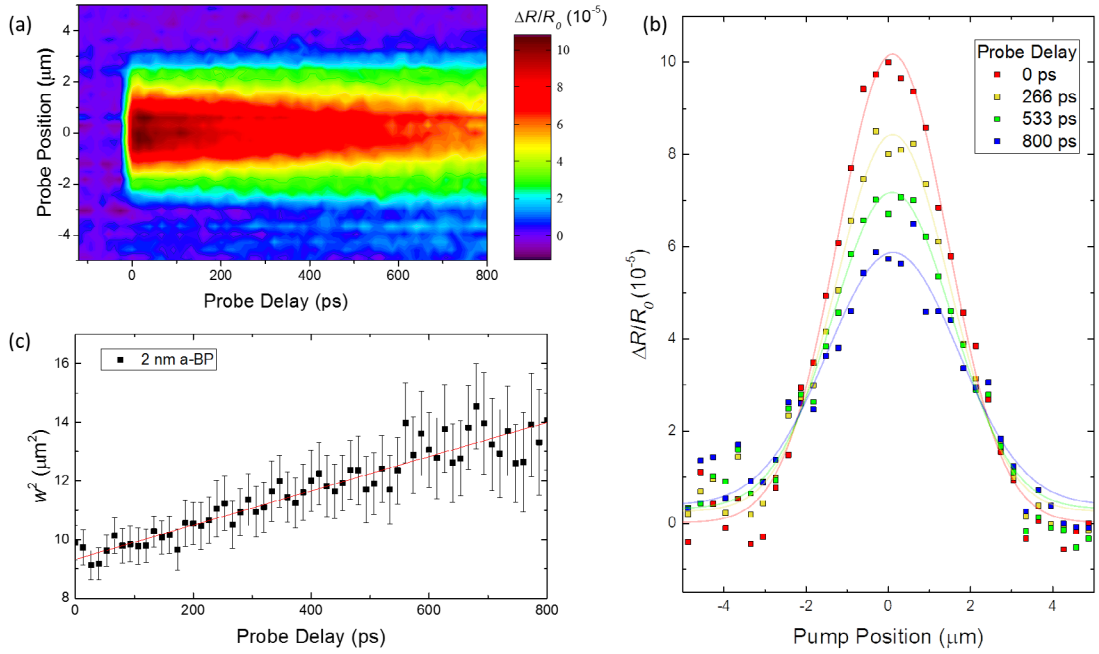

Figure 3. Exciton diffusion in the 2 nm a-BP ultrathin film measured by spatially resolved differential reflection. (a) Spatiotemporal differential reflection signal. (b) Spatial Gaussian profiles for different delay times. (c) The squared width of the Gaussian profiles as a function of the probe delay. The data is fit with a linear function in order to extract the diffusion coefficient from the slope.

more, by using the measured exciton lifetime of 400 ps, we obtain a diffusion length of $\sqrt{D\tau} = 450$ nm.

The superior exciton transport property of a-BP makes it an attractive amorphous material for optoelectronic applications. It is also interesting to compare the exciton transport with charge carrier transport in a-BP, which is relevant for electronic applications. Using the measured D and Einstein's relation, $\mu/e = D/k_B t$, where μ, e, and k_B are the mobility, the elementary charge, and Boltzmann constant, respectively, one can deduced an exciton mobility of about 200 $cm^2 V^{-1} s^{-1}$. This value is about one order of magnitude larger than charge carrier mobilities deduced from transport measurements [30]. The higher exciton mobility could be attributed to its relatively smaller scattering rate with piezoelectric phonons and charge impurities, since excitons do not have a net charge.

Similar experiments were also performed on the 5 nm and 10 nm a-BP films, with the same pump and probe photon energies of 1.57 and 0.80 eV, respectively. Figure 4(a) shows the differential reflection signal measured for a-BP ultrathin film samples with thicknesses of 2 (black squares), 5 (red squares), and 10 nm (blue squares), respectively. It can be clearly seen that the signals from thicker samples are significantly smaller. Similar to crystalline BP, we expect the band gap of a-BP to decrease with increasing the thickness. The 0.80 eV probe is tuned to the optical band gap of the 2 nm sample, and hence is expected to couple to higher energy states where the transient absorption is expected to be smaller. The deduced carrier lifetimes are similar to the 2 nm sample. The small difference could be attributed to sample-to-sample variation.

Finally, we attempted to measure the exciton diffusion coefficient in the 5- and 10 nm samples with the spatially resolved differential reflection measurements. These results are shown in figures 4(b) and (c). The squared width, found by fitting the spatiotemporal data with Gaussian functions for the different probe delays times, is shown in figure 4(d). The results from the 2 nm sample (black squares) is also plotted for comparison. As before, all three datasets were linearly fit in order to extract the diffusion coefficients from the respective slopes. It can clearly be seen that the slope decreases with thickness of a-BP. Excitons were found to diffuse in the 5 nm film with a diffusion coefficient of 3.4 ± 0.4 $cm^2 s^{-1}$. This is reasonably consistent with the 2 nm sample, considering sample-to-sample variations. Finally, the diffusion coefficient of excitons in the 10 nm sample is not measurable, which could be attributed to the small differential reflection signal of the sample.

4. Conclusion

We have shown that large area and uniform atomic layers of amorphous black phosphorus synthesized at low temperature possess a surprisingly high exciton diffusion coefficient and long exciton lifetime. Temporally and spatially resolved pump-probe measurements revealed that in ultrathin films of 2 nm the exciton in-plane diffusion coefficient is about 5 $cm^2 s^{-1}$, which is at least two orders of magnitude larger than amorphous silicon and corresponds to an exciton moblity of about 200 $cm^2 V^{-1} s^{-1}$. Combined with a long lifetime of about 400 ps, the exciton diffusion length reaches 450 nm. The results show

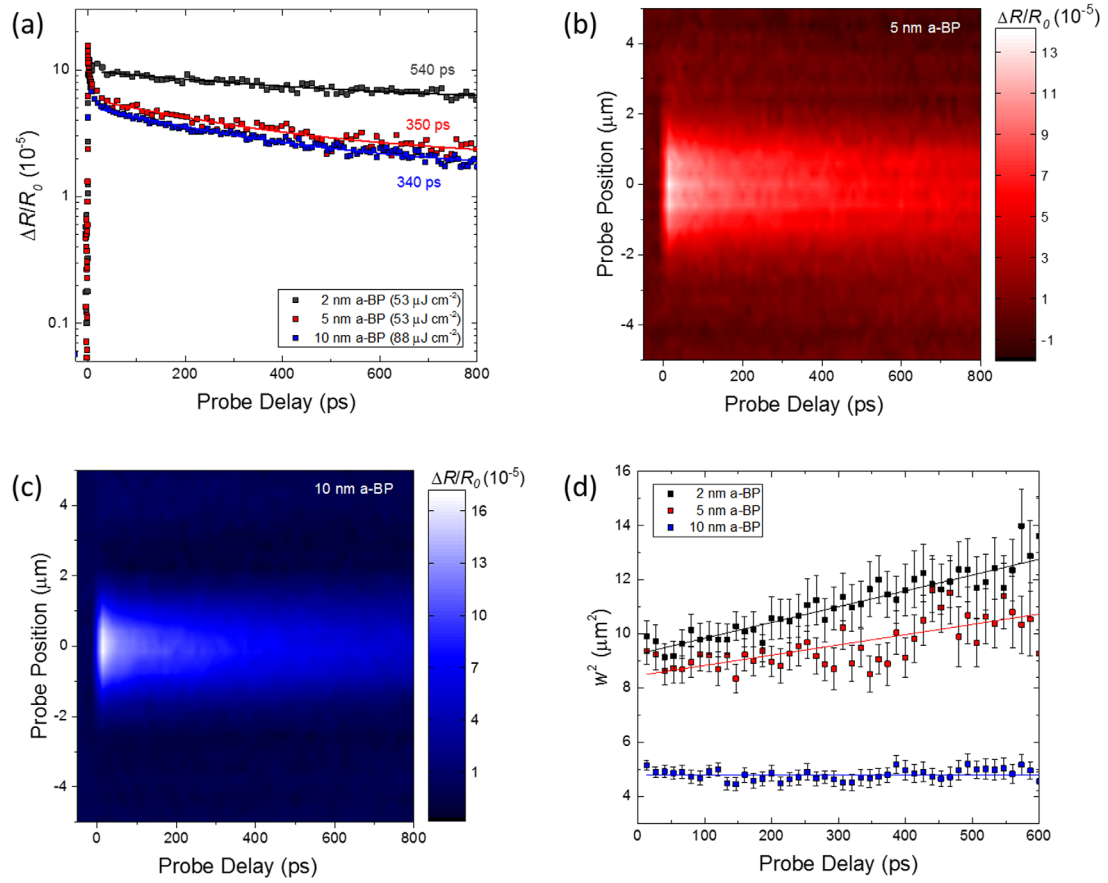

Figure 4. Differential reflection and exciton diffusion in the 5- and 10 nm a-BP ultrathin films (a) Differential reflection of the 2-, 5-, and 10 nm a-BP thin films plotted on a log scale versus relative probe delay. (b) Spatiotemporal differential reflection signal of the 5 nm a-BP film (c) Spatiotemporal differential reflection signal of the 10 nm a-BP film (d) The squared width of the Gaussian profiles as a function of the probe delay for the 2-, 5-, and 10 nm a-BP films. Each dataset is fit with a linear function in order to extract the diffusion coefficient from the slope.

that two-dimensional amorphous black phosphorus has potential for less expensive, better performing optoelectronic devices.

Acknowledgment

This material is partially based upon work supported by the National Science Foundation of USA under Award Nos. DMR-1505852 and IIA-1430493. This work was financially supported by the PolyU grants (1-ZE14 and 1-ZVGH) and the Research Grants Council (RGC) of Hong Kong (Project No. PolyU 153030/15P).

References

[1] Shah A, Torres P, Tscharner R, Wyrsch N and Keppner H 1999 *Science* **285** 692–8
[2] Lecomber P G, Spear W E and Ghaith A 1979 *Electron. Lett.* **15** 179–81
[3] Nomura K, Ohta H, Takagi A, Kamiya T, Hirano M and Hosono H 2004 *Nature* **432** 488–92
[4] Idota Y, Kubota T, Matsufuji A, Maekawa Y and Miyasaka T 1997 *Science* **276** 1395–7
[5] Suslick K S, Choe S B, Cichowlas A A and Grinstaff M W 1991 *Nature* **353** 414–6
[6] Smith R D L, Prevot M S, Fagan R D, Zhang Z P, Sedach P A, Siu M K J, Trudel S and Berlinguette C P 2013 *Science* **340** 60–3
[7] Mak K F and Shan J 2016 *Nat. Photon.* **10** 216–26
[8] Novoselov K S, Mishchenko A, Carvalho A and Castro Neto A H 2016 *Science* **353** 461
[9] Bhimanapati G R *et al* 2015 *ACS Nano* **9** 11509–39
[10] Zhong L *et al* 2016 *2D Mater.* **3** 042001
[11] Batmunkh M, Bat-Erdene M and Shapter J G 2016 *Adv. Mater.* **28** 8586–617
[12] Liu H, Neal A T, Zhu Z, Luo Z, Xu X, Tomanek D and Ye P D 2014 *ACS Nano* **8** 4033–41
[13] Favron A, Gaufres E, Fossard F, Phaneuf-L'Heureux A L, Tang N Y, Levesque P L, Loiseau A, Leonelli R, Francoeur S and Martel R 2015 *Nat. Mater.* **14** 826–32
[14] Li L K *et al* 2016 *Nat. Nanotechnol.* **11** 593–7
[15] Das S, Zhang W, Demarteau M, Hoffmann A, Dubey M and Roelofs A 2014 *Nano Lett.* **14** 5733–9
[16] Liang L, Wang J, Lin W, Sumpter B G, Meunier V and Pan M 2014 *Nano Lett.* **14** 6400–6
[17] Zhang S, Yang J, Xu R, Wang F, Li W, Ghufran M, Zhang Y. W, Yu Z, Zhang G, Qin Q and Lu Y 2014 *ACS Nano* **8** 9590–6
[18] Wang X M, Jones A M, Seyler K L, Tran V, Jia Y C, Zhao H, Wang H, Yang L, Xu X D and Xia F N 2015 *Nat. Nanotechnol.* **10** 517–21
[19] Yuan H T *et al* 2015 *Nat. Nanotechnol.* **10** 707–13
[20] Youngblood N, Chen C, Koester S J and Li M 2015 *Nat. Photon.* **9** 247–52
[21] Li L, Yu Y, Ye G J, Ge Q, Ou X, Wu H, Feng D, Chen X H and Zhang Y 2014 *Nat. Nanotechnol.* **9** 372–7

[22] Qiao J, Kong X, Hu Z X, Yang F and Ji W 2014 *Nat. Commun.* **5** 4475
[23] Du Y, Liu H, Deng Y and Ye P D 2014 *ACS Nano* **8** 10035–42
[24] Xia F, Wang H and Jia Y 2014 *Nat. Commun.* **5** 4458
[25] Liu H, Neal A T, Si M W, Du Y C and Ye P D 2014 *IEEE Electron. Dev. Lett.* **35** 795–7
[26] Das S, Demarteau M and Roelofs A 2014 *ACS Nano* **8** 11730–8
[27] Na J, Lee Y T, Lim J A, do K H, Kim G T, Choi W K and Song Y W 2014 *ACS Nano* **8** 11753–62
[28] Wood J D, Wells S A, Jariwala D, Chen K S, Cho E, Sangwan V K, Liu X, Lauhon L J, Marks T J and Hersam M C 2014 *Nano Lett.* **14** 6964–70
[29] He J, He D, Wang Y, Cui Q, Bellus M Z, Chiu H Y and Zhao H 2015 *ACS Nano* **9** 6436–42
[30] Yang Z, Hao J, Yuan S, Lin S, Yau H M, Dai J and Lau S P 2015 *Adv. Mater.* **27** 3748–54
[31] Li W, Yang Z, Li M, Jiang Y, Wei X, Zhong X, Gu L and Yu Y 2016 *Nano Lett.* **16** 1546–53
[32] Ceballos F and Zhao H 2016 *Adv. Funct. Mater.* https://doi.org/10.1002/adfm.201604509
[33] Nie Z, Long R, Sun L, Huang C C, Zhang J, Xiong Q, Hewak D W, Shen Z, Prezhdo O V and Loh Z H 2014 *ACS Nano* **8** 10931–40
[34] Sun D, Wu Z K, Divin C, Li X B, Berger C, de Heer W A, First P N and Norris T B 2008 *Phys. Rev. Lett.* **101** 157402
[35] Ruzicka B A, Kumar N, Wang S, Loh K P and Zhao H 2011 *J. Appl. Phys.* **109** 084322
[36] Zhao H, Moehl S, Wachter S and Kalt H 2002 *Appl. Phys. Lett.* **80** 1391
[37] Ceballos F, Cui Q, Bellus M Z and Zhao H 2016 *Nanoscale* **8** 11681–8
[38] Thilagam A 2016 *J. Appl. Phys.* **120** 124306
[39] Kumar N, Cui Q, Ceballos F, He D, Wang Y and Zhao H 2014 *Phys. Rev.* B **89** 125427
[40] Sun D, Rao Y, Reider G A, Chen G, You Y, Brezin L, Harutyunyan A R and Heinz T F 2014 *Nano Lett.* **14** 5625–9
[41] Yuan L and Huang L B 2015 *Nanoscale* **7** 7402–8
[42] Poellmann C, Steinleitner P, Leierseder U, Nagler P, Plechinger G, Porer M, Bratschitsch R, Schuller C, Korn T and Huber R 2015 *Nat. Mater.* **14** 889–93
[43] Ferrari A C, Meyer J C, Scardaci V, Casiraghi C, Lazzeri M, Mauri F, Piscanec S, Jiang D, Novoselov K S, Roth S and Geim A K 2006 *Phys. Rev. Lett.* **97** 187401
[44] Gu Q, Schiff E A, Grebner S, Wang F and Schwarz R 1996 *Phys. Rev. Lett.* **76** 3196–9
[45] Haken U, Hundhausen M and Ley L 1995 *Phys. Rev.* B **51** 10579–90
[46] Wang F and Schwarz R 1994 *Appl. Phys. Lett.* **65** 884–6